Nanoscale Advances

ROYAL SOCIETY OF CHEMISTRY

PAPER

View Article Online
View Journal | View Issue

Cite this: *Nanoscale Adv.*, 2020, **2**, 888

Ultrahigh photo-stable all-inorganic perovskite nanocrystals and their robust random lasing†

Liuli Yang,[a] Ting Wang,[a] Qiuhong Min,[a] Chaojie Pi,[a] Fan Li,[b] Xiao Yang,[b] Kongzhai Li,[c] Dacheng Zhou,[a] Jianbei Qiu,[a] Xue Yu *[a] and Xuhui Xu *[a]

Photo-instability has prevented further commercialization of all-inorganic perovskite nanocrystals (NCs) in the field of high-power optoelectronics. Here, an accelerated transformation process from non-luminescent Cs_4PbBr_6 to $CsPbBr_3$ NCs with bright green emission is explored with irradiation at 365 nm during water-triggered structural transformation. The photoelectric field provided by the photon energy of 365 nm promotes the rapid stripping of CsBr and atomic reconstruction, contributing to the production of ultrahigh photo-stable defect-free $CsPbBr_3$ NCs. The robust emission output of the as-obtained $CsPbBr_3$ NCs is well preserved even when recorded after 160 min. Moreover, a long-term stable random lasing could be achieved when excited using an ~800 nm femtosecond laser for at least 8.6×10^7 laser shots. Our results not only elucidate the photo-induced accelerated phase transformation process of the all-inorganic perovskites, but also open up opportunities to synthesize highly stable $CsPbBr_3$ NCs for their practical application in photovoltaics and optoelectronics.

Received 12th December 2019
Accepted 15th January 2020

DOI: 10.1039/c9na00775j

rsc.li/nanoscale-advances

Introduction

All-inorganic perovskite materials ($CsPbX_3$ with X = Br, I, or Cl) have garnered considerable attention owing to their intriguing applications in the field of optoelectronics.[1] However, halide perovskites are extremely susceptible to undergoing aggressive degradation upon exposure to H_2O, heating, and UV illumination.[2] Compared with a multitude of studies on their instability upon heating in a moist environment,[3–5] the light sensitivity of halide perovskite nanostructures remains largely unexplored. Particularly, light-induced instability of the photoelectric properties cannot be overlooked because the indispensable light irradiation induces the aggregation of perovskite NCs to form undesired defect states or structural changes, which fundamentally lead to a decline in photoelectric properties.[6] From this perspective, exploring the detailed phase transformation mechanism under light irradiation could be expected to be the key to solving the light instability problem of all-inorganic perovskite NCs. McNeill's group found that the defect concentration of $MAPbBr_3$ (MA = methylammonium) material increases after high power illumination, owing to the degradation of the I-rich domains.[7] Moreover, Zeng *et al.* reported the photon-induced structural transition between orthorhombic and tetragonal phases in $CsPbBr_3$ under above-bandgap (2.36 eV) irradiation.[8] Schaller's group proposed a reversible and light-driven orthorhombic-to-cubic phase transition at an excitation flux threshold greater than 0.34 mJ cm^{-2}.[9] Kim and co-workers demonstrated that structural variations occur with the assistance of light induction.[10] Although it is accepted that halide perovskites tend to actively respond to light through changes in their structure and properties, there are still gaps in their stability disturbance and the understanding of their structural transformation involving photons.[11,12]

Structural transformation and atomic stripping have been observed during water-involved synthesis processes. Yin *et al.* reported a water-triggered transformation of Cs_4PbBr_6 to $CsPbBr_3$ NCs by stripping CsBr through an interfacial reaction with water in a different phase.[13] Turedi *et al.* employed water to directly transform films of $CsPbBr_3$ to stable $CsPb_2Br_5$ under $PbBr_2$ rich conditions.[14] Moreover, Xia *et al.* discussed that the post-synthetic water treatment of $CsPbBr_3$ NCs can remove the surface atoms to enhance stability.[15] From these studies, dealing with the issue of phase transformation within a moist environment is critical to the acquisition of stabilized perovskites. On the basis of the abovementioned reports, the stability of perovskites should not be examined with the exposure to light or moisture alone, especially for practical application, since both of them induce the degradation of perovskites fundamentally.

[a]*Faculty of Materials Science and Engineering, Kunming University of Science and Technology, Wenchang Road, Kunming, 650093, China. E-mail: yuyu6593@126.com; xuxuh07@126.com*

[b]*Department of Materials Science and Engineering, Nanchang University, 999 Xuefu Avenue, Nanchang 330031, China*

[c]*State Key Laboratory of Complex Nonferrous Metal Resources Clean Utilization, Kunming University of Science and Technology, Kunming 650093, China*

† Electronic supplementary information (ESI) available: Size distribution of Cs_4PbBr_6 NCs and $CsPbBr_3$ NCs, pictures of CsBr, Cs_4PbBr_6 and $CsPbBr_3$, XRD of CsBr and products obtained at different reaction stages, HRTEM images, FFT images, IFFT images of single nanocrystals, TEM images of Cs_4PbBr_6 NCs and $CsPbBr_3$ NCs, band structure and density of states of Cs_4PbBr_6, and PL emission spectra of $CsPbBr_3$ NCs. See DOI: 10.1039/c9na00775j

In this work, we explored the 365 nm-irradiation effect on the water-triggered structural transformation of the as-obtained perovskite Cs_4PbBr_6 NCs and found an accelerated phase transformation process producing defect-free $CsPbBr_3$. The as-obtained $CsPbBr_3$ NCs show ultrahigh-stability against light and moisture, compared with those prepared through a hot-injection method. The cooperative effect of water and photon energy on the phase transformation from Cs_4PbBr_6 to $CsPbBr_3$ inhibits the formation of defects fundamentally. Hence, we unambiguously demonstrate that the ultrahigh photo-stability of the defect free $CsPbBr_3$ NCs provides the possibility for the construction of a long-term stable lasing gain medium.

Experimental section

Chemicals

Cesium carbonate (Cs_2CO_3, Aladdin, 99.99%), lead(II) bromide ($PbBr_2$, Aladdin, 99.999%), oleylamine (OLA, 80–90%), octadecene (ODE, Aladdin, 90%), oleic acid (OA, Aladdin, AR), and toluene (Chengdu Chemical, AR) were used. All chemicals were used without any further purification.

Synthesis and purification of Cs_4PbBr_6 NCs

The synthesis process was performed in air without any pre-dried chemicals or solvents. In a typical synthesis procedure, $PbBr_2$ (0.1 mmol) was dissolved in 0.5 mL ODE, 1 mL OA and 1.5 mL OLA in a 20 mL vial on a hotplate set at 100 °C. After $PbBr_2$ was completely dissolved (at around 120 °C), the vial was moved to a room temperature (RT) hotplate. When the temperature reached 80 °C, 0.6 mL of Cs–OA (0.8 g Cs_2CO_3 dissolved in 8 mL OA in a 20 mL vial on a hotplate set to 190 °C) was quickly injected. 30 seconds after the injection, the reaction mixture was quickly cooled down to 50 °C in an ice-water bath for the next purification process. The NCs were directly washed *via* centrifugation 3 times (at 6000 rpm for 15 min), followed by re-dispersion in 5 mL toluene.

Synthesis of water-induced $CsPbBr_3$ NCs

The synthesis process was conducted under ambient conditions. 125 μL deionized water was directly injected into 1 mL Cs_4PbBr_6 solution and shaken.

Synthesis of water- and irradiation-induced $CsPbBr_3$ NCs

The synthesis process was conducted under ambient conditions. 125 μL deionized water was directly injected into 1 mL Cs_4PbBr_6 solution and shaken slightly. The mixture was irradiated under light (2 mW cm^{-2}) of different wavelengths (none, 254 nm, 365 nm, 468 nm, and 600 nm) for 20 min. The final $CsPbBr_3$ solution was re-dispersed in 1 mL toluene.

Preparation of photo-responsive samples

The photocurrent of Cs_4PbBr_6 NCs was measured on an electrochemical workstation by the traditional three-electrode method consisting of a working electrode (photoelectron anode), platinum foil as a counter electrode, and a saturated calomel electrode (SCE) as a reference electrode. The electrolyte solution used in the photocurrent measurement was sodium sulfate solution. The working electrode was prepared by a drop-coating method. The Cs_4PbBr_6 solution was coated onto FTO conducting glass. After the resulting glass was air-dried, the working electrode was obtained.

Characterization

X-ray diffraction (XRD) patterns were obtained using a D8 Focus diffractometer (Bruker) with Cu-Kα radiation ($\lambda = 0.15405$ nm) in the 2θ range from 10° to 50°. The photo-luminescence (PL) spectra of the samples were recorded by using a FLAME-S-XR1-ES spectrophotometer (Shenzhen Yanyou Instrument Ltd, Shenzhen, China). UV-Vis absorption spectra of $CsPbBr_3$ were recorded using a HITACHI U-4100 UV-Vis-NIR spectrophotometer with an integrating sphere in diffuse-reflectance mode. The particle morphology and size were studied using field emission transmission electron microscopy (TEM) and high-resolution transmission electron microscopy (HRTEM), carried out using a TECNAI G2F30 S-TWIN operating at 300 kV. The macroscopic structures of $CsPbBr_3$ (before and after laser emission) were examined by using a Quanta 200FEG scanning electron microscope (SEM) equipped with an energy dispersive spectrometer (EDS). The samples were prepared by drop casting diluted NC suspensions onto 400 mesh ultrathin/holey carbon-coated copper grids for conventional TEM imaging and HRTEM imaging. Micro-frequency Raman measurements were carried out using an argon laser with a continuous wave ($k = 785$ nm) as the excitation source (Renishaw inVia, Gloucestershire, UK). The spectra were recorded with an acquisition time of 1 s and accumulation number of 60. The photocurrent–voltage characteristics were measured by using a Keithley 2400 sourcemeter under 365 nm-irradiation. Fourier transform infrared spectroscopy (FTIR) spectra were measured by using a Nicolet iS 10 Fourier transform infrared spectrometer. X-ray Photoelectron Spectroscopy (XPS) analysis was carried out using a Thermo fisher Scientific K-Alpha and an Al-Kα X-ray source ($h\nu = 1486.6$ eV) with a 400 μm spot size and 30 eV pass energy. For the random lasing measurement, a homemade micro-PL system (OlympusBX-52 microscope and a 20× 0.8 NA objective lens) was used to focus an 800 nm femtosecond laser beam on $CsPbBr_3$ NCs. A Ti:sapphire femtosecond laser (Coherent Libra) integrated with an optical parametric amplifier (Coherent OPerA Solo), which generates femtosecond pulses (50 fs, 1 kHz), was used as the excitation source. $CsPbBr_3$ NCs were placed inside a low-temperature (77 K) chamber under laser spot excitation. The received optical signal emitted from the sample was coupled to a conventional CCD camera for recording the near-field image and attached to a monochromator (Princeton SpectraPro 2750 integrated with a ProEM EMCCD camera with spectral resolution less than 0.1 nm) for spectral analysis.

Results and discussion

X-ray diffraction (XRD) patterns were recorded to indicate the phase transformation from Cs_4PbBr_6 to $CsPbBr_3$ NCs with and

without UV irradiation, as shown in Fig. 1. The as-obtained Cs_4PbBr_6 NCs *via* the hot-injection method are gradually transformed to $CsPbBr_3$ with the emergence of a peak at 15° after soaking in water for 8 hours. After 48 hours, all the $CsPbBr_3$ diffraction peaks appear, which means the phase transition is achieved, as presented in Fig. 1a. This was consistent with the previously reported water-triggered process.[13] An identical phase transformation is observed in Fig. 1b. Nevertheless, the appearance of the diffraction peak of $CsPbBr_3$ at 15° is recorded after 3 hours for the sample soaking in water under 365 nm-irradiation, and the pure phase of $CsPbBr_3$ is obtained after 5 hours. This suggests that an accelerated phase transformation occurs with the intervention of 365 nm-irradiation. Fig. 1c and d, respectively, present the corresponding transmission electron microscopy (TEM) images of these samples recorded during the phase transformation process. The TEM images in Fig. 1c1 and d1 demonstrate the good dispersity of the as-obtained Cs_4PbBr_6 NCs with an average size of 20 nm and faint luminescence. The morphology of these NCs changes fundamentally, revealed by TEM images, respectively, recorded after 1 and 1/3 hours under 365 nm-irradiation, as shown in Fig. 1c2 and d2. For the 365 nm-irradiated sample more CsBr NCs[16] precipitate than for its counterpart without the participation of photons. Meanwhile, the green emission is observed obviously as shown in the inset of Fig. 1c2 and d2, demonstrating the appearance of $CsPbBr_3$.[13] Fig. 1c3 and d3, respectively, present the coexistence of Cs_4PbBr_6 and $CsPbBr_3$ NCs with definitely different morphologies, and the luminescence intensity of the green emission originating from $CsPbBr_3$ NCs is greatly improved. The single-phase of the $CsPbBr_3$ sample with quasi-square particles is finally obtained after 48 hours (Fig. 1c4) and 5 hours (Fig. 1d4), respectively, with and without the irradiation at 365 nm. Notably, the good dispersity of $CsPbBr_3$ NCs under 365 nm-irradiation is identical to that of the non-irradiated ones for the water triggered phase transformation process, and the distribution of particle size of both the samples is around 20 nm in mean size (Fig. S1†). Here, it can be inferred that light irradiation promotes the fracture of the soft structure of Cs_4PbBr_6 and thereby accelerates the phase transformation from Cs_4PbBr_6 to $CsPbBr_3$ NCs. Moreover, the luminescence intensity of the green emission originating from $CsPbBr_3$ during the phase transformation is recorded and exhibited in Fig. 1e and f, which further illustrates the shortened reaction time of phase change and the improved optical performance of the sample under 365 nm-irradiation.

In situ Raman spectra of the as-obtained samples are shown in Fig. 2a and b, which present the structural changes of the non-

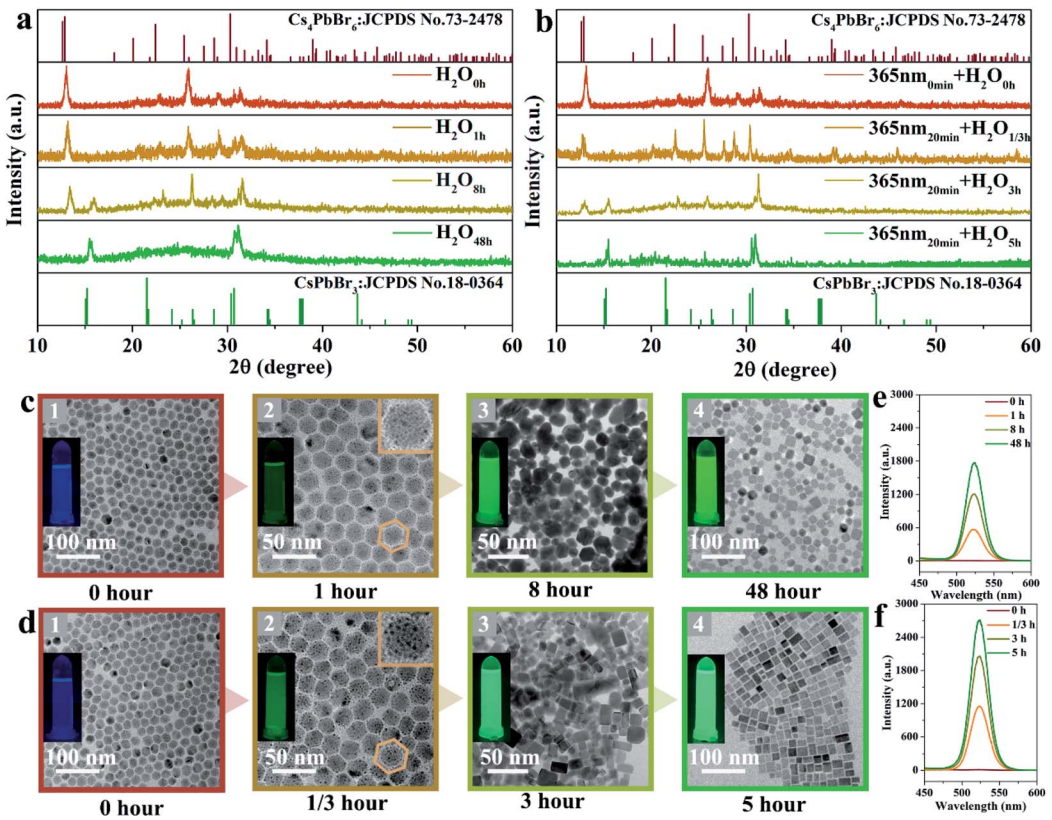

Fig. 1 Phase transformation of $CsPbBr_3$ NCs. XRD patterns of the corresponding samples undergoing the phase transformation process in water without (a) and with the irradiation at 365 nm (b). TEM images recorded during the phase transformation process in water without (c) and with 365 nm-irradiation (d), the insets on the left present the photographs of the corresponding samples under 365 nm excitation, and the insets of (c2) and (d2) in the upper right corner are the topographical maps of the corresponding nanoparticles. The PL spectra of the corresponding samples recorded during the phase transformation without (e) and with 365 nm-irradiation (f) under 365 nm excitation.

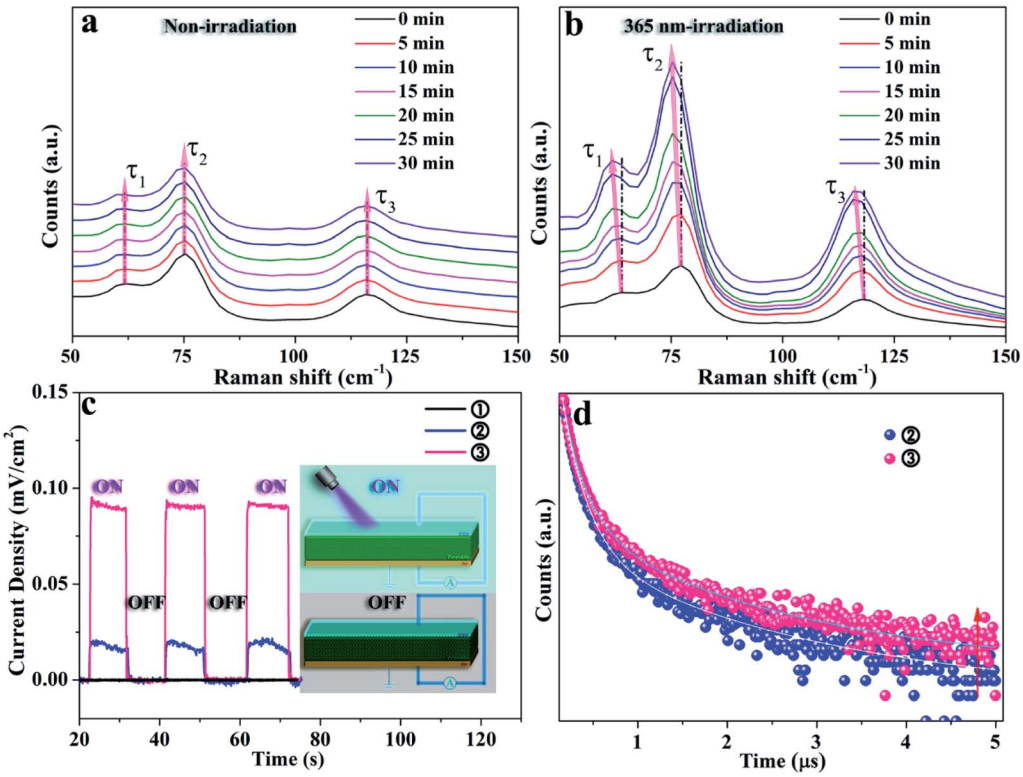

Fig. 2 Raman profiles of the non-irradiated (a) and 365 nm-irradiated (b) samples with a prolonged recording time, transient photocurrent curves of samples undergoing different phase transformations (c), with the inset showing the corresponding schematic diagram of the device structure, and PL decay dynamics of the 365 nm-irradiated sample (d) (sample ①: water treatment for 0 min, without 365 nm-irradiation; ②: water treatment for 20 min, without 365 nm-irradiation; ③: water treatment for 20 min, with 365 nm-irradiation for 20 min).

irradiated and the 365 nm-irradiated samples, respectively. The first peak τ_1 around 63 cm^{-1} and the third peak τ_3 around 118 cm^{-1} are assigned to the vibration mode of Cs ions, while the second peak τ_2 around 77 cm^{-1} is important evidence for the distortion of the vibrations of the $[PbX_6]^{4-}$ octahedron.[17] It has been determined that the shift of the Raman peak related to lattice disorder and strain leads to the photo-striction motion in 3D perovskites.[18] As shown in Fig. 2a, the sample with non-irradiation shows insignificant change of Raman spectra both in the peak position for the above mentioned different vibration modes and in the Raman intensity during the prolonged recording time. It indicates that no apparent structural variation occurs in the non-irradiated sample within the initial 30 min. In contrast, the characteristic vibration peaks of the 365 nm-irradiated sample show a continuous red-shift depending on the irradiation time. Specifically, the red-shifts of Raman peaks τ_1, τ_2 and τ_3 are observed from 63 to 61 cm^{-1}, 77 to 75 cm^{-1}, and 118 to 116 cm^{-1}, respectively, after 30 min of 365 nm-irradiation. It unambiguously demonstrates that the lattice geometry of the Pb–Br octahedron and Cs ions changes. Furthermore, the increased ratio of I_{τ_2}/I_{τ_1} from 1.54 to 1.61 in Fig. 2b indicates the decreased amount of cesium ions which is attributed to the strain induced by the increasing disorder of crystal lattices during the phase transformation process.[19] It is accepted that irradiation can lead to thermal effects and photoelectric fields, both of which can have an effect on the structure of the light-sensitive crystal.[20–23] Fig. S2† illustrates the effect of ambient temperature on the emission intensity of these samples during phase transformation. There is no significant increase in the emission intensity of these samples heated at different temperatures, indicating that thermal energy provided by heat-treatment is not a key factor in promoting phase transformation. Fig. 2c presents the photocurrent curve of the samples under 365 nm-light (60 mW cm^{-2}). The resulting photocurrent shows three distinct ON/OFF cycles under irradiation switching. As shown in Fig. 2c, sample ① of Cs_4PbBr_6 NCs possesses poor photo-response due to the high exciton binding energy originating from the unique 0D structure.[24,25] Photocurrent signals appear in samples ② and ③, which is believed to be accomplished along with the appearance of $CsPbBr_3$ NCs. A further increase in the amount of $CsPbBr_3$ NCs contributes to a drastic increase in the photocurrent intensity as sample ③ displayed. The appearance of photocurrent density confirms the generation of a photoelectric field, and the enhancement of photocurrent confirms that the irradiation could accelerate phase transformation effectively, as $CsPbBr_3$ NCs have a highly sensitive photo-response than Cs_4PbBr_6 NCs.[26,27] Therefore, it can be speculated that a photoelectric field is generated in the sample under 365 nm irradiation. The existence of the photoelectric field accelerates the formation of $CsPbBr_3$ NCs, which subsequently contributes to a stronger photocurrent as can be seen from Fig. 2c, contributing to the acquisition of defect free $CsPbBr_3$ NCs

from the phase transformation. Besides, time-resolved PL decay curves of samples ② and ③ are measured and plotted in Fig. 2d, which indicate that their average PL lifetime is 135 and 272 ns, respectively. The increase of the carrier lifetime from 135 to 272 ns confirms that the presence of 365 nm irradiation contributes to the production of the photocurrent field, and thereby accelerates the structural change of the perovskite.[28]

The comparative experiments on the photo-response properties of the perovskites under irradiation with different wavelengths show that 365 nm irradiation is beneficial to the stable optical output, which is believed to be due to the reduction of the surface ligands attached on sub-$CsPbBr_3$ NCs as illustrated in Fig. S3.† The photon energy of 365 nm is believed to provide a photoelectric field as discussed above, where the interaction between the organic ligands and the $[PbBr_6]^{4-}$ octahedron in Cs_4PbBr_6 NCs is certainly weakened, resulting in ligand stripping and accelerating the phase transition process.[8,29] Thus, we propose the reaction schematic diagram of the phase transformation under irradiation with different wavelengths as shown in Fig. S4a,† and the corresponding mechanism diagram is shown in Fig. S4b.† Furthermore, we plot the optical properties of these samples under irradiation with the optimal absorption bands of 365 and 468 nm as displayed in Fig. S5a and b.† It further demonstrates that the phase transition

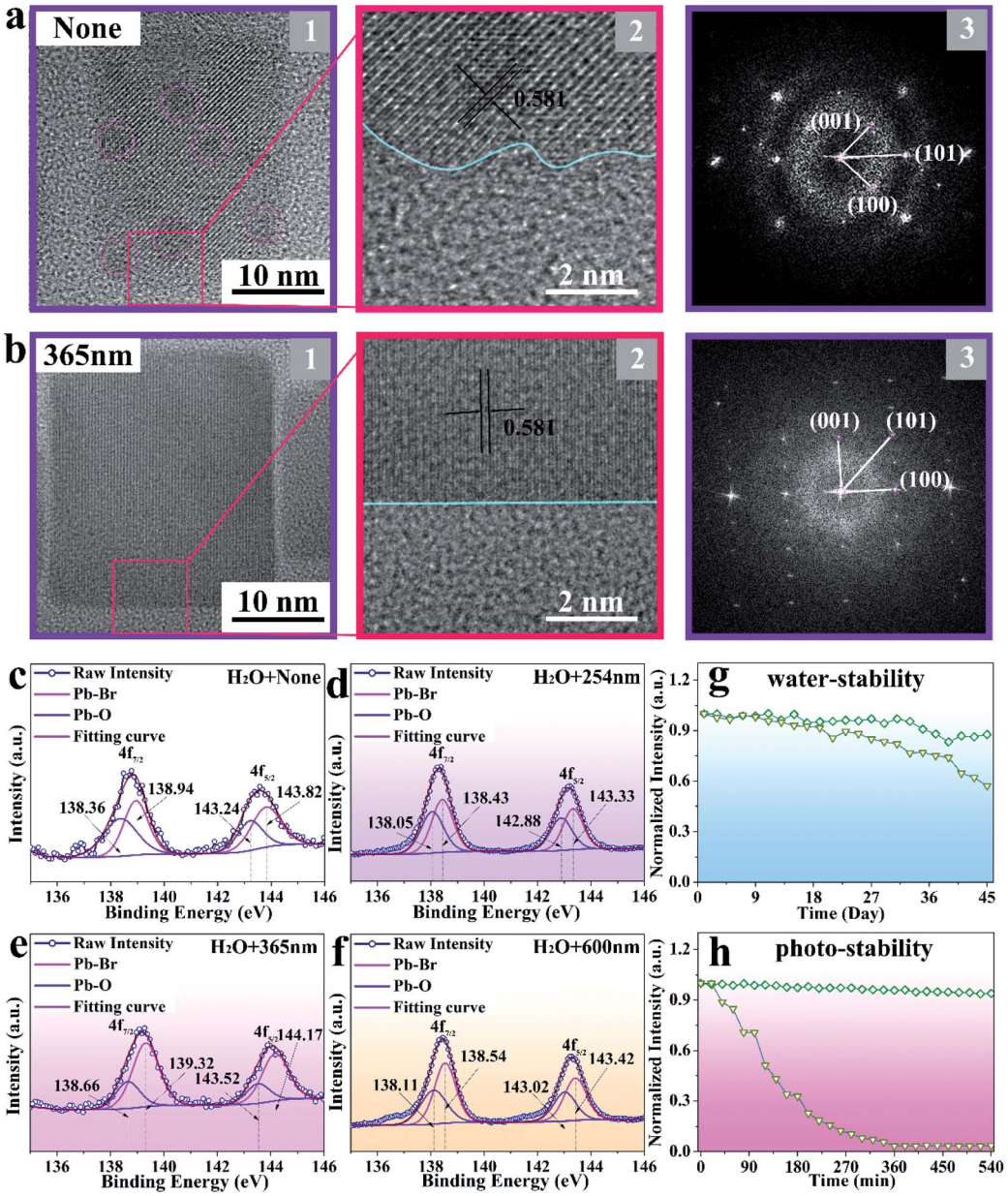

Fig. 3 HRTEM images of the non-irradiated (a1) and 365 nm-irradiated (b1) $CsPbBr_3$ NCs, local HRTEM images (a2 and b2), and the corresponding FFT patterns (a3 and b3) obtained from the HRTEM images. XPS peak fitting of Pb 4f spectra of $CsPbBr_3$ NCs treated with non-irradiation (c), 254 nm (d), 365 nm (e) and 600 nm (f) irradiation. Normalized emission intensity of non-irradiated (triangles) and 365 nm-irradiated (squares) $CsPbBr_3$ NCs in an aqueous environment (g) and under 365 nm irradiation (h), respectively.

process can be accelerated without damaging the structure under irradiation with the optimal absorption band.

The HRTEM and fast Fourier transform (FFT) images shown in Fig. 3a and b further reveal the same lattice spacing of 0.581 nm for the obtained sample under non-irradiation and 365 nm-irradiation treatment, respectively, which is in good agreement with the (100) crystal plane of monoclinic $CsPbBr_3$ NCs. However, it should be noticed that the external defects and internal black dots observed in non-irradiated $CsPbBr_3$ NCs disappeared after 365 nm-irradiation treatment, and the sample presents a regular surface and good crystallinity. To analyze the detailed information of the defects, XPS measurement is employed to represent the peaks of Pb–Br and Pb–oleate species. As displayed in Fig. 3c–f, the binding energy of Pb $4f_{7/2}$ and $4f_{5/2}$ appears around 138.5 and 143.5 eV, respectively. Comparing the relative amounts of the Pb–oleate species in the samples obtained through different treatments (none, 254 nm, 365 nm, and 600 nm-irradiation), it is found that $CsPbBr_3$ NCs treated with 365 nm-irradiation exhibit the least number of defects[30] (a quantitative comparison of the defects is shown in Table S1†), which fundamentally contributes to the enhancement of emission intensity.

The stability of perovskite NCs is critical for their long-term operation. As plotted in Fig. 3g, the 365 nm-irradiated $CsPbBr_3$ NCs exhibit high emission intensity endurance (92%) after exposing them to 125 μL water for 45 days, while the emission intensity of non-irradiated $CsPbBr_3$ NCs decreased to 55% of its initial intensity. Moreover, the sample irradiated at 365 nm presents a striking photo-stability (93%) when immersed in 125 μL water and exposed to 365 nm-illumination for 540 min, while the non-irradiated $CsPbBr_3$ NCs degrade immediately (Fig. 3h).[15] The corresponding mechanism diagrams are displayed in Fig. S6.† After immersing the two samples in 125 μL water, the structure is not destroyed due to the protection of the ligand. However, the structure of the non-irradiated sample is destroyed due to the existence of a large number of defects when exposed to 365 nm irradiation, while that of the irradiated sample remains intact.

The employed high-energy pumping to realize the upconversion lasers requires superior long-term stability of samples. Here, the performance of the upconversion lasing of the 365 nm-irradiated $CsPbBr_3$ NCs is studied specifically. As displayed in Fig. 4a and b, the $CsPbBr_3$ NCs, with an even size and

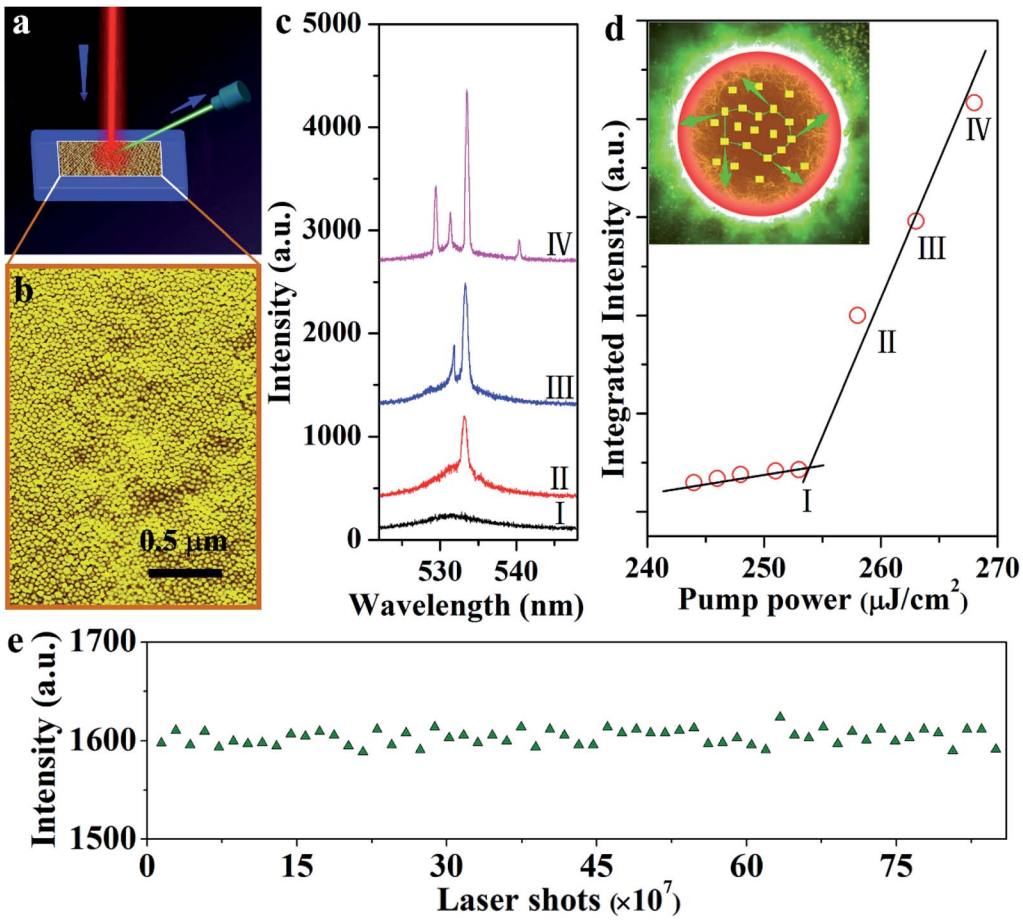

Fig. 4 PL and lasing characteristics of the $CsPbBr_3$ NC laser. Schematic of $CsPbBr_3$ NCs on a silicon substrate pumped *via* an 800 nm femtosecond laser (a). The corresponding SEM image of the sample is shown in (b). Emission spectra of the $CsPbBr_3$ NCs with different pump powers, showing the transition from amplified spontaneous emission to lasing (c). Integrated emission intensity as a function of pump density showing the lasing threshold (~254 μJ cm^{-2}) (d). Inset: Schematic diagram of the formation of a closed loop path for light through recurrent scattering in the samples. Lasing intensity for $CsPbBr_3$ NCs measured above ($1.5P_{th}$) the lasing threshold (e).

uniform distribution, emit green lasing when excited using an 800 nm femtosecond laser beam. A broad spontaneous emission band centered at ~532 nm is observed under 800 nm excitation at 77 K (Fig. 4c). As the pump power increases, the number of sharp peaks increases and the intensity increases simultaneously. When the pump power goes up to 2.5 μJ cm^{-2}, the sharp peak exhibits an extremely narrow line width of 0.3 nm. In addition, the pump-dependence of spectrally integrated emission intensity shows obvious threshold behavior, as shown in Fig. 4d. These results are consistent with the behavior of random lasers: as the pump power increases, a broad spontaneous emission peak appears first, followed by a laser mode at a higher pumping rate.[31] In the case of high gain and strong scattering, recurrent scattering events occur, thereby forming closed loop paths when the pump intensity reaches above the threshold (the inset of Fig. 4d). Since different closed loop paths formed at different angles, the laser emission spectra change with the different angles (Fig. S7a†). The plot of excitation area (A_{th}) *versus* the corresponding excitation threshold (P_{th}) satisfies the relationship (Fig. S7b†):

$$A_{th}^{2/3} \approx kP_{th}^{-1}$$

where k is a constant.[32] Meanwhile, the lasing intensity of the $CsPbBr_3$ NCs is monitored under the constant pumping of the laser with a pump density of $1.5P_{th}$ as shown in Fig. 4e and S7c,† and the random lasing is able to withstand more than 8.6×10^7 excitation cycles (longer than 24 hours) with an intact morphology, suggesting the ultrahigh photo-stability.

Conclusion

In conclusion, a light-induced transformation strategy was developed for obtaining high photo-stability $CsPbBr_3$ NCs with the cooperation of water. A photoelectric field, provided by a photon energy of 365 nm, promotes the rearrangement of atoms in water and accelerates the phase transformation drastically. Photo-stability and water resistance results suggest that the 365 nm-irradiated $CsPbBr_3$ NCs are ultra-high stable to support a random lasing output. Overall, we conclude that the use of light induces an accelerated phase transformation of an all-inorganic perovskite, which produces highly stable $CsPbBr_3$ NCs with a low number of defects, providing a robust optical output for practical application.

Author contributions

The authors contributed equally to this work.

Conflicts of interest

There are no conflicts to declare.

Acknowledgements

This work was financially supported by the National Natural Science Foundation of China (11664022, 61965012), the Reserve Talents Project of Yunnan Province (2017HB011), the Yunnan Ten Thousand Talents Plan Young & Elite Talents Project (YNWR-QNBJ-2018-295, YNWR-QNBJ-2018-325), the Excellent Youth Project of Yunnan Province Applied Basic Research Project (2019FI001), and the Foundation of Yunnan Province (2019HC016).

References

1 S. Colella, M. Mazzeo, A. Rizzo, G. Gigli and A. Listorti, The Bright Side of Perovskites, *J. Phys. Chem. Lett.*, 2016, **7**, 4322–4334.
2 E. T. Hoke, D. J. Slotcavage, E. R. Dohner, A. R. Bowring, H. I. Karunadasa and M. D. McGehee, Reversible photo-induced trap formation in mixed-halide hybrid perovskites for photovoltaics, *Chem. Sci.*, 2015, **6**(1), 613–617.
3 E.-P. Yao, Z. Yang, L. Meng, P. Sun, S. Dong, Y. Yang and Y. Yang, High-Brightness Blue and White LEDs based on Inorganic Perovskite Nanocrystals and their Composites, *Adv. Mater.*, 2017, **29**(23), 1606859.
4 X. Li, Y. Wu, S. Zhang, B. Cai, Y. Gu, J. Song and H. Zeng, $CsPbX_3$ Quantum Dots for Lighting and Displays: Room-Temperature Synthesis, Photoluminescence Superiorities, Underlying Origins and White Light-Emitting Diodes, *Adv. Funct. Mater.*, 2016, **26**(15), 2435–2445.
5 H. Cho, Y. H. Kim, C. Wolf, H. D. Lee and T. W. Lee, Improving the Stability of Metal Halide Perovskite Materials and Light-Emitting Diodes, *Adv. Mater.*, 2018, **30**(42), e1704587.
6 G. Abdelmageed, L. Jewell, K. Hellier, L. Seymour, B. Luo, F. Bridges, J. Z. Zhang and S. Carter, Mechanisms for light induced degradation in $MAPbI_3$ perovskite thin films and solar cells, *Appl. Phys. Lett.*, 2016, **109**, 233905.
7 S. Ruan, M.-A. Surmiak, Y. Ruan, D. P. McMeekin, H. Ebendorff-Heidepriem, Y.-B. Cheng, J. Lu and C. R. McNeill, Light induced degradation in mixed-halide perovskites, *J. Mater. Chem. C*, 2019, **7**(30), 9326–9334.
8 J. Xue, D. Yang, B. Cai, X. Xu, J. Wang, H. Ma, X. Yu, G. Yuan, Y. Zou, J. Song and H. Zeng, Photon-Induced Reversible Phase Transition in $CsPbBr_3$ Perovskite, *Adv. Funct. Mater.*, 2019, **29**(13), 1807922.
9 M. S. Kirschner, B. T. Diroll, P. Guo, S. M. Harvey, W. Helweh, N. C. Flanders, A. Brumberg, N. E. Watkins, A. A. Leonard, A. M. Evans, M. R. Wasielewski, W. R. Dichtel, X. Zhang, L. X. Chen and R. D. Schaller, Photoinduced, reversible phase transitions in all-inorganic perovskite nanocrystals, *Nat. Commun.*, 2019, **10**(1), 504.
10 D. Kim, J. S. Yun, P. Sharma, D. S. Lee, J. Kim, A. M. Soufiani, S. Huang, M. A. Green, A. W. Y. Ho-Baillie and J. Seidel, Light- and bias-induced structural variations in metal halide perovskites, *Nat. Commun.*, 2019, **10**(1), 444.
11 Y. Wang, L. Gao, Y. Yang, Y. Xiang, Z. Chen, Y. Dong, H. Zhou, Z. Cai, G.-C. Wang and J. Shi, Nontrivial strength of van der Waals epitaxial interaction in soft perovskites, *Phys. Rev. Mater.*, 2018, **2**(7), 076002.
12 J. K. Sun, S. Huang, X. Z. Liu, Q. Xu, Q. H. Zhang, W. J. Jiang, D. J. Xue, J. C. Xu, J. Y. Ma, J. Ding, Q. Q. Ge, L. Gu,

X. H. Fang, H. Z. Zhong, J. S. Hu and L. J. Wan, Polar Solvent Induced Lattice Distortion of Cubic $CsPbI_3$ Nanocubes and Hierarchical Self-Assembly into Orthorhombic Single-Crystalline Nanowires, *J. Am. Chem. Soc.*, 2018, **140**(37), 11705–11715.

13 L. Wu, H. Hu, Y. Xu, S. Jiang, M. Chen, Q. Zhong, D. Yang, Q. Liu, Y. Zhao, B. Sun, Q. Zhang and Y. Yin, From Nonluminescent Cs_4PbX_6 (X = Cl, Br, I) Nanocrystals to Highly Luminescent $CsPbX_3$ Nanocrystals: Water-Triggered Transformation through a CsX-Stripping Mechanism, *Nano Lett.*, 2017, **17**(9), 5799–5804.

14 B. Turedi, K. J. Lee, I. Dursun, B. Alamer, Z. Wu, E. Alarousu, O. F. Mohammed, N. Cho and O. M. Bakr, Water-Induced Dimensionality Reduction in Metal-Halide Perovskites, *J. Phys. Chem. C*, 2018, **122**(25), 14128–14134.

15 Y. Liu, F. Li, Q. Liu and Z. Xia, Synergetic Effect of Postsynthetic Water Treatment on the Enhanced Photoluminescence and Stability of $CsPbX_3$ (X = Cl, Br, I) Perovskite Nanocrystals, *Chem. Mater.*, 2018, **30**(19), 6922–6929.

16 L. Yang, T. Wang, Q. Min, B. Liu, Z. Liu, X. Fan, J. Qiu, X. Xu, J. Yu and X. Yu, High Water Resistance of Monoclinic $CsPbBr_3$ Nanocrystals Derived from Zero-Dimensional Cesium Lead Halide Perovskites, *ACS Omega*, 2019, **4**(3), 6084–6091.

17 D. M. Calistru, L. Mihut, S. Lefrant and I. Baltog, Identification of the symmetry of phonon modes in $CsPbCl_3$ in phase IV by Raman and resonance-Raman scattering, *J. Appl. Phys.*, 1997, **82**(11), 5391–5395.

18 T. C. Wei, H. P. Wang, T. Y. Li, C. H. Lin, Y. H. Hsieh, Y. H. Chu and J. H. He, Photostriction of $CH_3NH_3PbBr_3$ Perovskite Crystals, *Adv. Mater.*, 2017, **29**(35), 1701789.

19 M. Liao, B. Shan and M. Li, *In Situ* Raman Spectroscopic Studies of Thermal Stability of All-Inorganic Cesium Lead Halide ($CsPbX_3$, X = Cl, Br, I) Perovskite Nanocrystals, *J. Phys. Chem. Lett.*, 2019, **10**(6), 1217–1225.

20 A. Masunov, J. J. Dannenberg and R. H. Contreras, C-H Bond-Shortening upon Hydrogen Bond Formation: Influence of an Electric Field, *J. Phys. Chem. A*, 2001, **105**(19), 4737–4740.

21 W. Choe, V. K. Pecharsky, A. O. Pecharsky, K. A. Gschneidner Jr, V. G. Young Jr and G. J. Miller, Making and breaking covalent bonds across the magnetic transition in the giant magnetocaloric material $Gd_5(Si_2Ge_2)$, *Phys. Rev. Lett.*, 2000, **84**(20), 4617.

22 D. A. Davis, A. Hamilton, J. Yang, L. D. Cremar, D. Van Gough, S. L. Potisek, M. T. Ong, P. V. Braun, T. J. Martinez, S. R. White, J. S. Moore and N. R. Sottos, Force-induced activation of covalent bonds in mechanoresponsive polymeric materials, *Nature*, 2009, **459**(7243), 68–72.

23 J. W. Mintmire, B. I. Dunlap and C. T. White, Are fullerene tubules metallic?, *Phys. Rev. Lett.*, 1992, **68**(5), 631–634.

24 S. Seth and A. Samanta, Fluorescent Phase-Pure Zero-Dimensional Perovskite-Related Cs_4PbBr_6 Microdisks: Synthesis and Single-Particle Imaging Study, *J. Phys. Chem. Lett.*, 2017, **8**(18), 4461–4467.

25 H. Zhang, Q. Liao, Y. Wu, J. Chen, Q. Gao and H. Fu, Pure zero-dimensional Cs_4PbBr_6 single crystal rhombohedral microdisks with high luminescence and stability, *Phys. Chem. Chem. Phys.*, 2017, **19**(43), 29092–29098.

26 J. H. Cha, J. H. Han, W. Yin, C. Park, Y. Park, T. K. Ahn, J. H. Cho and D. Y. Jung, Photoresponse of $CsPbBr_3$ and Cs_4PbBr_6 Perovskite Single Crystals, *J. Phys. Chem. Lett.*, 2017, **8**(3), 565–570.

27 Y. Dong, Y. Zou, J. Song, Z. Zhu, J. Li and H. Zeng, Self-powered fiber-shaped wearable omnidirectional photodetectors, *Nano Energy*, 2016, **30**, 173–179.

28 S. Gao, B. Gu, X. Jiao, Y. Sun, X. Zu, F. Yang, W. Zhu, C. Wang, Z. Feng, B. Ye and Y. Xie, Highly Efficient and Exceptionally Durable CO_2 Photoreduction to Methanol over Freestanding Defective Single-Unit-Cell Bismuth Vanadate Layers, *J. Am. Chem. Soc.*, 2017, **139**(9), 3438–3445.

29 D. Yang, X. Li, W. Zhou, S. Zhang, C. Meng, Y. Wu, Y. Wang and H. Zeng, $CsPbBr_3$ Quantum Dots 2.0: Benzenesulfonic Acid Equivalent Ligand Awakens Complete Purification, *Adv. Mater.*, 2019, e1900767.

30 Y. Wu, C. Wei, X. Li, Y. Li, S. Qiu, W. Shen, B. Cai, Z. Sun, D. Yang, Z. Deng and H. Zeng, In Situ Passivation of $PbBr_6^{4-}$ Octahedra toward Blue Luminescent $CsPbBr_3$ Nanoplatelets with Near 100% Absolute Quantum Yield, *ACS Energy Lett.*, 2018, **3**(9), 2030–2037.

31 H. Cao, Y. G. Zhao, S. T. Ho, E. W. Seelig, Q. H. Wang and R. P. H. Chang, Random Laser Action in Semiconductor Powder, *Phys. Rev. Lett.*, 1999, **82**(11), 2278.

32 S. F. Yu, C. Yuen, S. P. Lau and H. W. Lee, Zinc oxide thin-film random lasers on silicon substrate, *Appl. Phys. Lett.*, 2004, **84**(17), 3244–3246.